Article

# Electrokinetic Transport in Microchannels with Random Roughness

Moran Wang, and Qinjun Kang

*Anal. Chem.*, **2009**, 81 (8), 2953-2961• DOI: 10.1021/ac802569n • Publication Date (Web): 20 March 2009

*Anal. Chem.* **2009,** *81,* 2953–2961

# Electrokinetic Transport in Microchannels with Random Roughness

**Moran Wang* and Qinjun Kang**

*Computational Earth Science Group (EES-16), Los Alamos National Laboratory, Los Alamos, New Mexico 87545*

**We present a numerical framework to model the electrokinetic transport in microchannels with random roughness. The three-dimensional microstructure of the rough channel is generated by a random generation-growth method with three statistical parameters to control the number density, the total volume fraction, and the anisotropy characteristics of roughness elements. The governing equations for the electrokinetic transport are solved by a high-efficiency lattice Poisson−Boltzmann method in complex geometries. The effects from the geometric characteristics of roughness on the electrokinetic transport in microchannels are therefore modeled and analyzed. For a given total roughness volume fraction, a higher number density leads to a lower fluctuation because of the random factors. The electroosmotic flow rate increases with the roughness number density nearly logarithmically for a given volume fraction of roughness but decreases with the volume fraction for a given roughness number density. When both the volume fraction and the number density of roughness are given, the electroosmotic flow rate is enhanced by the increase of the characteristic length along the external electric field direction but is reduced by that in the direction across the channel. For a given microstructure of the rough microchannel, the electroosmotic flow rate decreases with the Debye length. It is found that the shape resistance of roughness is responsible for the flow rate reduction in the rough channel compared to the smooth channel even for very thin double layers, and hence plays an important role in microchannel electroosmotic flows.**

When the characteristic length scale of a system is down to micro- or nanometers, the interfacial phenomena become very important.[1,2] The electrokinetic transport, as a classical interfacial phenomenon discovered more than 200 years ago, now plays a fundamental role for a better understanding of liquid flow mechanism through microchannels,[3] and hence for optimal design and operation of microsystems, such as Laboratory-on-a-chip devices[4,5] and micro fuel cells.[6−8] In the mean time, electrokinetic flow has become one of the most important non-mechanical actuating techniques in microfluidics, widely used for pumping,[9−12] mixing,[13−15] and separating,[16] and so on, because of its excellent scalability, low dispersion, and ease of control.[4,10,13,17] Therefore, analysis and modeling of electrokinetic transport in microchannels have recently received a lot of attention.[18−25]

Almost all surfaces have certain degree of roughness, either incurred during fabrication process or because of the adsorption/adhesion of other species such as macromolecules. Although it is well-known that the electrokinetic flow is sensitive to the surface properties,[26] little attention has been paid to the effects of surface roughness on electrokinetic transport because of its complexity, especially for random roughness in microchannels.[27]

Dukhin and Derjaguin[28] may be the first ones who performed systematic theoretical studies on roughness effects on electrokinetic flows. They introduced two critical length scales to characterize the problem: the Debye length, which is defined as the thickness of the electrical double layer, and the characteristic length of surface roughness. For a thin double layer case where the Debye length is much smaller than the surface roughness height, the electroosmotic flow near the concave-convex portion

* To whom correspondence should be addressed. E-mail: mwang@lanl.gov (M.W.), qkang@lanl.gov.

(1) Squires, T. M.; Quake, S. R. *Rev. Mod. Phys.* **2005**, *77*, 977–1026.
(2) Schoch, R. B.; Han, J.; Renaud, P. *Rev. Mod. Phys.* **2008**, *80*, 839–883.
(3) Li, D. Q. *Electrokinetics in microfluidics*; Academic: Oxford, 2004.
(4) Stone, H. A.; Stroock, A. D.; Ajdari, A. *Annu. Rev. Fluid Mech.* **2004**, *36*, 381–411.
(5) Gui, L.; Ren, C. L. *Langmuir* **2008**, *24*, 2938–2946.
(6) Chrzanowski, W.; Wieckowski, A. *Langmuir* **1998**, *14*, 1967–1970.
(7) Wang, C. Y. *Chem. Rev.* **2004**, *104*, 4727–4765.
(8) Buie, C. R.; Kim, D.; Litster, S.; Santiago, J. G. *Electrochem. Solid State Lett.* **2007**, *10*, B196–B200.
(9) Chen, C. H.; Santiago, J. G. *J. Microelectromech. Syst.* **2002**, *11*, 672–683.
(10) Yao, S. H.; Santiago, J. G. *J. Colloid Interface Sci.* **2003**, *268*, 133–142.
(11) Wang, M.; Wang, J. K.; Chen, S. Y.; Pan, N. *J. Colloid Interface Sci.* **2006**, *304*, 246–253.
(12) Bazant, M. Z.; Squires, T. M. *Phys. Rev. Lett.* **2004**, *92*, 066101.
(13) Oddy, M. H.; Santiago, J. G.; Mikkelsen, J. C. *Anal. Chem.* **2001**, *73*, 5822–5832.
(14) Biddiss, E.; Erickson, D.; Li, D. Q. *Anal. Chem.* **2004**, *76*, 3208–3213.
(15) Wang, J. K.; Wang, M. R.; Li, Z. X. *Mod. Phys. Lett. B* **2005**, *19*, 1515–1518.
(16) Wong, P. K.; Wang, T. H.; Deval, J. H.; Ho, C. M. *IEEE-ASME Trans. Mechatron.* **2004**, *9*, 366–376.
(17) Li, D. Q. *Encyclopedia of Microfluidics and Nanofluidics*; Springer Verlag: New York, 2008.
(18) Dutta, P.; Beskok, A. *Anal. Chem.* **2001**, *73*, 1979–1986.
(19) Li, D. Q. *Colloids Surf., A* **2001**, *195*, 35–57.
(20) Li, B. M.; Kwok, D. Y. *Langmuir* **2003**, *19*, 3041–3048.
(21) Fu, L. M.; Lin, J. Y.; Yang, R. J. *J. Colloid Interface Sci.* **2003**, *258*, 266–275.
(22) Guo, Z. L.; Zhao, T. S.; Shi, Y. *J. Chem. Phys.* **2005**, *122*, 144907.
(23) Hlushkou, D.; Seidel-Morgenstern, A.; Tallarek, U. *Langmuir* **2005**, *21*, 6097–6112.
(24) Wang, J. K.; Wang, M.; Li, Z. X. *J. Colloid Interface Sci.* **2006**, *296*, 729–736.
(25) Huang, K. D.; Yang, R. J. *Electrophoresis* **2006**, *27*, 1957–1966.
(26) Butt, H. J.; Graf, K.; Kappl, M. *Physics and chemistry of interfaces*; Wiley-VCH: Weinheim, 2003.
(27) Vourdas, N.; Tserepi, A.; Boudouvis, A. G.; Gogolides, E. *Microelectron. Eng.* **2008**, *85*, 1124–1127.
(28) *Electrokinetic phenomena*; Dukhin, S. S., Derjaguin, B. V., Eds.; Wiley: New York, 1974.

10.1021/ac802569n CCC: $40.75 
Published on Web 03/20/2009

of the rough surface is essentially the same as that near a smooth surface, and the Smoluchowski equation is therefore valid. In this case, the electroosmotic flow in a rough channel can thus be predicted by the standard linear models. When the Debye length is comparable to the roughness height, the linearized models fail to describe the electrokinetic transport. Especially when the Debye length is much larger than the roughness size, the effective charge density on the rough surfaces may be higher than that on the corresponding smooth surfaces because of the increased area caused by the roughness.[26]

Thanks to the rapid development of computer and computational techniques, a few numerical approaches have been applied to modeling and predicting the electrokinetic transport in rough microchannels. Hu et al.[29−31] studied the electroosmotic flow in microchannels with three-dimensional (3D) rectangular roughness elements using a finite-volume-based numerical model within a thin Debye length limit. Finite element method and analysis have been employed as well to investigate the electroosmotic flow in microchannels with two-dimensional sinusoidal roughness.[32,33] Recently, a lattice Poisson−Boltzmann method (LPBM) has been proposed as an efficient solver for the strongly nonlinear equations governing electrokinetic flows in microchannels[24] and has been used to investigate the two-dimensional rectangular roughness and cavitation effects.[34] Up to now the electrokinetic flows in microchannels with random roughness have never been studied to the best knowledge of the authors.

There are two challenges to model the electrokinetic flows in microchannels with random roughness. The first one is how to describe the complex geometries of random roughness in microchannels. In most cases the roughness in a real microchannel caused by manufacture or macromolecule adsorption is uncontrollable, which means that the roughness geometry features, such as position, shape, and size, are irregular and random. Since the electrokinetic flows are sensitive to surface characteristics, any imitation with regular geometry for roughness may lead to inaccurate predictions and analysis for a real system. However there is not yet an effective way in the existing literature for digitalizing the complex geometries of random roughness in microchannels. Second, solving the governing equations efficiently for electrokinetic flow in complex geometries is formidable. The coupled electrostatic, hydrodynamic, and mass transport problem subject to complex geometrical boundary conditions represented by the solid−liquid interface in randomly rough channels requires huge or even unacceptable computational resources for the traditional partial differential equation (PDE) solvers, such as the finite difference method (FDM) and the finite element method (FEM). The difficulty mainly comes from two aspects: the strong nonlinearity of the governing equations and the irregularity of the random structures. The former may cause the classical PDE solvers to be unstable or even disconvergent, while the latter will lead to a requirement for extreme grid refinements in the computational domain especially near the roughness. This computational difficulty in traditional PDE solvers thus has limited modeling and analysis of electrokinetic flow to very simple geometries.

Facing these challenges, we are aiming to (1) build up a numerical framework for modeling electrokinetic transport in microchannels with random roughness; (2) analyze the effects of roughness geometry on the electrodynamic and hydrodynamic transport in microchannels. The results will be compared with the existing theoretical analysis and/or numerical data.

## MATHEMATICAL MODELS

Consider an $N$-component Newtonian electrolyte flowing with a velocity $\mathbf{u}(\mathbf{r},t)$ in microchannels with no polarization or chemical reactions. Let $\psi(\mathbf{r},t)$ be the electric potential prevailing within the solution where $\mathbf{r}$ is the position vector. The flux $\mathbf{J}_i$ of the $i$th ion species, composing the solute, is given by the following constitutive equation:[26,35]

$$\mathbf{J}_i = -D_i\nabla n_i - \frac{ez_iD_in_i}{kT}\nabla\psi + n_i\mathbf{u} \tag{1}$$

where $n_i$ is the number density of the $i$th ion species, $z_i$ the $i$th ion algebraic valence, $e$ the absolute charge of electron, $D_i$ the ion's diffusivity, $k$ the Boltzmann constant, and $T$ the absolute temperature. The ionic flux $\mathbf{J}_i$ and the concentration $n_i$ obey the equation

$$\frac{\partial n_i}{\partial t} + \nabla\cdot\mathbf{J}_i = 0 \tag{2}$$

For an incompressible laminar electroosmotic flow, the movement of fluid is governed by the continuity and momentum equations:

$$\nabla\cdot\mathbf{u} = 0 \tag{3}$$

$$\rho\frac{\partial\mathbf{u}}{\partial t} + \rho\mathbf{u}\cdot\nabla\mathbf{u} = \mu\nabla^2\mathbf{u} + \mathbf{F} \tag{4}$$

where $\rho$ is the fluid density, and $\mu$ the dynamic fluid viscosity. $\mathbf{F}$ can be any kind of body force but here we only consider the driving force from the electric field. In general, the electric force in electrokinetic fluids may include the Lorentz force associated with an external applied electric field, the force caused by the electromagnetic susceptibility, and the intermolecular electric attraction.[24] In the present contribution, we consider the very slow quasi-steady-state- electrokinetic flow in microchannels so that all other electromagnetic forces are negligible compared to the static electric force. Therefore the driving force is simplified as

$$\mathbf{F} = \rho_e\mathbf{E} \tag{5}$$

where $\rho_e$ is the net charge density and $\mathbf{E}$ is the electric field strength vector. The net charge density $\rho_e$ can be expressed as

$$\rho_e = \sum_i ez_in_i \tag{6}$$

The electric potential distribution is governed by the Poisson equation


(29) Hu, Y. D.; Werner, C.; Li, D. Q. *Anal. Chem.* **2003**, *75*, 5747–5758.
(30) Hu, Y. D.; Werner, C.; Li, D. Q. *J. Colloid Interface Sci.* **2004**, *280*, 527–536.
(31) Hu, Y. D.; Xuan, X. C.; Werner, C.; Li, D. Q. *Microfluid. Nanofluid.* **2007**, *3*, 151–160.
(32) Das, P. K.; Bhattacharjee, S. *J. Colloid Interface Sci.* **2004**, *273*, 278–290.
(33) Yang, D. Y.; Liu, Y. *Colloids Surf., A* **2008**, *328*, 28–33.
(34) Wang, M. R.; Wang, J. K.; Chen, S. Y. *J. Comput. Phys.* **2007**, *226*, 836–851.
(35) Lichtner, P. C. *Mater. Res. Soc. Symp. Proc.* **1995**, *353*, 117–130.

$$\nabla^2\psi = -\frac{\rho_e}{\varepsilon_r\varepsilon_0} = -\frac{1}{\varepsilon_r\varepsilon_0}\sum_{i=1}^{N} en_i z_i \tag{7}$$

where $\varepsilon_r$ is the dimensionless fluid dielectric constant and $\varepsilon_0$ the permittivity of a vacuum.

Equations 2−7 are the governing equations for electroosmosis in microchannels and can be solved subject to the following boundary conditions on the liquid−solid interface Ω

$$(\mathbf{v}\cdot\mathbf{J}_i)_\Omega = 0 \tag{8}$$

$$\mathbf{u}_\Omega = 0 \tag{9}$$

$$\psi_\Omega = \zeta \tag{10}$$

where $\mathbf{v}$ is the outer normal to Ω, and $\zeta$ the zeta potential.

When the ionic convection is negligible and the electric potential field is continuously derivable, eq 2 has a simple steady-state solution for dilute electrolyte solutions in which the ionic concentration $n_i$ falls into the Boltzmann distribution:

$$n_i = n_{i,\infty}\exp\left(-\frac{ez_i}{kT}\psi\right) \tag{11}$$

where $n_{i,\infty}$ is the bulk ionic number density. Substituting eq 11 into eq 7 yields the famous nonlinear Poisson−Boltzmann equation for electrokinetic flows:[36]

$$\nabla^2\psi = -\frac{1}{\varepsilon_r\varepsilon_0}\sum_i ez_i n_{i,\infty}\exp\left(-\frac{ez_i}{kT}\psi\right) \tag{12}$$

The present contribution solves the governing equations (3−6, 11, 12) subject to the boundary conditions eqs 8−10 by the numerical methods described in the next section.

## NUMERICAL METHODS

This section describes the numerical methods used to simulate electrokinetic flows in microchannels with random roughness, including a reproduction algorithm for 3D random roughness microstructures and a mesoscopic PDE solver for the multiphysical transport equations, the lattice Poisson−Boltzmann method.

**Reproduction of Random Roughness in 3D Microchannels.** The geometric characteristics of random roughness in microchannels are very complicated. Although the geometric details of each roughness element, such as shape, size, and connections, are quite random in a real microchannel, people can still measure and summarize essential statistical information of morphology and then generate an equivalent structure on a computer. The macroscopic statistical information of random roughness may include the following: the roughness position distribution, the roughness elements' shape and size, the anisotropy of roughness elements, and so on. The reproduced roughness microstructure may not have to be identical with the real one in every detail but should include the same main statistical macroscopic structure characteristics.

*Description of Algorithm.* No references have been found to reproduce the random roughness in microchannels because of its complexity. Our objective is to digitalize the rough channel geometry into a reasonable grid set. Inspired by the random generation-growth method for constructing random microstructures of porous media,[37,38] we develop a new method to reproduce microstructures of random roughness on upper and lower smooth walls in a 3D microchannel.

The main idea is to reproduce the rough microchannel geometry in a 3D digital grid matrix, with 0 representing the fluid and 1 the solid on each node. The initial state is a smooth straight channel, whose grid matrix is composed of all zeros (0) except the top and bottom walls. The roughness geometry is then reproduced by the random generation growth model described below.

(i) Randomly locate seeds of roughness elements on the upper and lower wall surfaces based on a roughness distribution probability, $s_d$. The value of $s_d$ cannot be greater than the total volume fraction of roughness, $V_R$, defined as the ratio of the total volume of roughness elements to the fluid volume for the original smooth channel. Each cell of both walls is assigned a random number by a uniform distribution function within (0, 1). The cell whose random number is no greater than $s_d$ will be chosen as a roughness element seed;

(ii) Grow every cell of the existing roughness elements to its neighboring fluid cells along its six possible directions (front, back, left, right, up and down) based on a given directional growth probability, $D_j$, where $j$ represents the direction. Again for each neighboring cell, a new random number will be assigned and the one whose random number is no greater than $D_j$, will become part of roughness. If the neighboring cell is already part of wall or roughness, it will remain in its state.

(iii) Repeat the growth process of (ii) until the total volume fraction of roughness elements reaches the given value $V_R$.

Thus the generated microstructure is controlled by the three statistical parameters, $s_d$, $D_j$ and $V_R$.

*Discussion on Parameters.* The roughness distribution probability, $s_d$, defined as the probability of a cell/grid on the walls to become a seed of roughness, is strongly related to the number density of roughness elements. For a given total roughness volume fraction $V_R$, the number density of roughness elements $n_R$ is related to $s_d$ as follows:

$$n_R = N_{wall}\cdot s_d / A_{wall} \tag{13a}$$

where $N_{wall}$ and $A_{wall}$ denote the total cell number and area of each wall, respectively. The average volume of each roughness element $\bar{V}_{r\_e}$ is

$$\bar{V}_{r\_e} = V_0 V_R/(2N_{wall}\cdot s_d) \tag{13b}$$

with $V_0$ representing the volume of the original smooth channel and $V_0V_R$ the total volume of the roughness elements.

The value of $s_d$ also controls the degree of structure details for a given volume fraction of roughness and grid systems. A smaller $s_d$ is required for a finer description of the microstructures, including shape and connections of the roughness elements.

The directional growth probability $D_j$, defined as the probability of a neighboring cell in the *j-th* direction to become a part of roughness elements, controls the degree of anisotropy.

(36) Honig, B.; A, N. *Science* **1995**, *268*, 1144–1149.

(37) Wang, M. R.; Wang, J. K.; Pan, N.; Chen, S. Y. *Phys. Rev. E* **2007**, *75*, 036702.

(38) Wang, M.; Chen, S. *J. Colloid Interface Sci.* **2007**, *314*, 264–273.

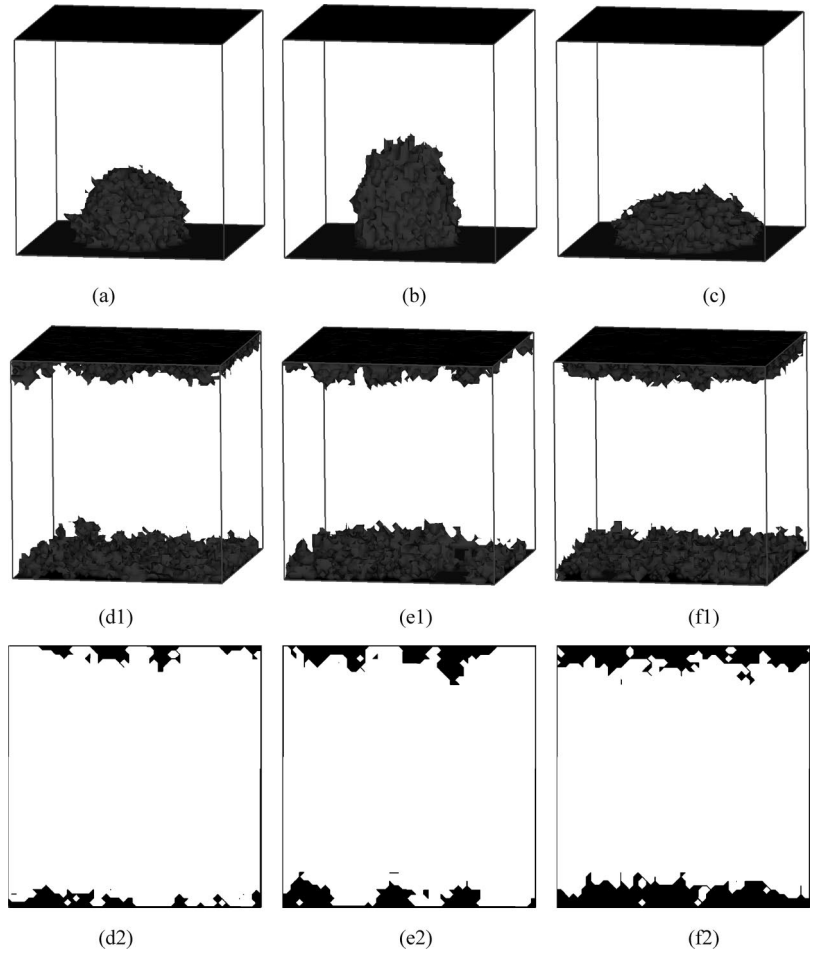


**Figure 1.** Generated 3D geometries for different parameters. Panels a−c show the single roughness element cases at the center of the lower wall at $V_R = 0.05$ where (a) $D_x:D_y:D_z = 1:1:1$; (b) $D_x:D_y:D_z = 1:1:4$; (c) $D_x:D_y:D_z = 4:4:1$. Panels d−f show the random roughness in 3D and *x*-*z* cross sections for different parameters: (d) $s_d = 0.03$ and $V_R = 0.06$; (e) $s_d = 0.01$ and $V_R = 0.06$; (f) $s_d = 0.03$ and $V_R = 0.1$.

Different from those for porous media,[38] there are only six growth directions (front, back, left, right, up and down) for roughness elements because any roughness cell has to be connected with other solid cells rather than stay isolated. We can obtain an "isotropic" structure of roughness elements by assigning each directional growth probability the same value. The so-called isotropic structure for a single roughness element is a half-spherical structure in statistics. We can vary the anisotropy of roughness structures by changing the ratio (not the absolute value) of the growth probabilities for different directions. Half-elliptical structures will be generated if the ratio $D_x:D_y:D_z$ does not equal unit, and the ratio of the mean radius ($\bar{R}_j$) is proportional to that of the square root of the growth probability: $\bar{R}_x:\bar{R}_y:\bar{R}_z = \sqrt{D_x}:\sqrt{D_y}:\sqrt{D_z}$.

*Examples.* To show the roughness shape changing with the directional growth probability, we first generate one single roughness element in the channel by placing only one seed on the center of the lower wall. Figure 1a−c shows three generated 3D geometries of one single roughness element on a grid system of $60 \times 60 \times 60$. The seed position is at the center of the lower wall. The stochastic characteristics of structures are depicted quite realistically in the figures. Figure 1a shows a half-sphere-like structure since the growth probabilities in all directions into the fluid are equal. The structure is therefore statistically isotropic from its seed position, which is the center of the half-sphere. Anisotropic structures are demonstrated in Figure 1b,c by changing the growth probability ratios. Half-ellipse-like structures are generated. When the growth probability in the *z* direction is four times of that in the other two directions, the *z*-directional mean radius is approximately two times of that in the other two directions, as shown in Figure 1b. The *z*-directional mean radius is half of that in the *x*- and *y*-directions if its growth probability is a quarter of the other ones (see Figure 1c). These results confirm that the characteristic length in each direction is proportional to the square root of its growth probability.

Panels d and f of Figure 1 show the effects of the roughness distribution probability and the roughness volume fraction on the geometries and connections in the rough microchannels. The roughness elements are supposed to be isotropic statistically. The $60 \times 60 \times 60$ grid is used and the locations of the *x*-*z* cross section profiles are randomly chosen. Comparisons between panels d and e of Figure 1 indicate that a larger roughness distribution probability leads to more roughness elements with a smaller averaged roughness element size for the same roughness volume fraction. A larger total roughness volume fraction results in larger roughness size and greater roughness connections according to Figure 1d,f.

**Lattice Poisson−Boltzmann Method.** After the rough channel is generated, the set of coupled hydrodynamic and electrodynamic governing equations for the electrokinetic flows subject

to the appropriate boundary conditions will be solved by the LPBM. This method combines an electric potential evolution method on discrete lattices to solve the nonlinear Poisson equation (lattice Poisson method) with a density evolution method on the same set of discrete lattices to solve the Boltzmann-BGK equation (lattice Boltzmann method).[24] The equations are only solved in the liquid phase, and the solid phase is silent and charged homogeneously on the surfaces.

*Evolution Equations.* Unlike conventional computational methods based on macroscopic continuum equations, the lattice Boltzmann method (LBM) employs the mesoscopic Boltzmann equation to determine macroscopic transport dynamics, and solves the governing equations by tracking distribution functions of particle packets on lattices.[39] For laminar flows driven by an external force, the Boltzmann-BGK equation with an external force term, $F$, is

$$\frac{\mathrm{D}f}{\mathrm{D}t} \equiv \partial_t f + (\xi\cdot\nabla)f = -\frac{f - f^{eq}}{\tau} + F \tag{14}$$

where $f \equiv f(x,\xi,t)$ is the single particle distribution function in the phase space $(x,\xi)$, $\xi$ the microscopic velocity, $\tau$ the relaxation time, $f^{eq}$ the Maxwell−Boltzmann equilibrium distribution, and $F$ the external force term which has the following form

$$F = \frac{3\mathbf{G}\cdot(\xi - \mathbf{u})}{c^2} f^{eq} \tag{15}$$

where $\mathbf{G}$ is the external force per unit mass,[40] $\mathbf{u}$ the fluid macroscopic velocity vector, and $c$ the lattice speed for mass transfer defined as $\delta_x/\delta_t$ with $\delta_x$ representing the lattice constant (grid size) and $\delta_t$ the time step.

The discrete density evolution equation can be written as

$$f_\alpha(\mathbf{r} + \mathbf{e}_\alpha\delta_t, t + \delta_t) - f_\alpha(\mathbf{r}, t) = -\frac{1}{\tau_\nu}[f_\alpha(\mathbf{r}, t) - f_\alpha^{eq}(\mathbf{r}, t)] + \delta_t F_\alpha \tag{16}$$

where $\mathbf{e}_\alpha$ denote the discrete velocities and for a 3D nineteen-speed (D3Q19) system,

$$\mathbf{e}_\alpha = \begin{cases} (0,0,0) & \alpha = 0 \\ (\pm1,0,0)c, (0 \pm 1,0)c, (0,0,\pm1)c & \alpha = 1 \text{ to } 6 \\ (\pm1,\pm1,0)c, (\pm1,0,\pm1)c, (0,\pm1,\pm1)c & \alpha = 7 \text{ to } 18 \end{cases} \tag{17}$$

and $\tau_\nu$ the dimensionless relaxation time which is a function of the fluid viscosity,

$$\tau_\nu = \frac{3\nu}{\delta_x c} + 0.5 \tag{18}$$

with $\nu$ representing the kinetic viscosity.

For the D3Q19 model, the density equilibrium distribution $f_\alpha^{eq}$ takes the following form

$$f_\alpha^{eq} = \omega_\alpha \rho\left[1 + 3\frac{\mathbf{e}_\alpha\cdot\mathbf{u}}{c^2} + 9\frac{(\mathbf{e}_\alpha\cdot\mathbf{u})^2}{2c^4} - \frac{3\mathbf{u}^2}{2c^2}\right] \tag{19}$$

with

$$\omega_\alpha = \begin{cases} 1/3 & \alpha = 0 \\ 1/18 & \alpha = 1 \text{ to } 6 \\ 1/36 & \alpha = 7 \text{ to } 18 \end{cases} \tag{20}$$

The external force in the discrete evolution equation is

$$F_\alpha = \frac{3\rho_e \mathbf{E}\cdot(\mathbf{e}_\alpha - \mathbf{u})}{\rho c^2} f_\alpha^{eq} \tag{22}$$

The macroscopic density and velocity can be calculated using

$$\rho = \sum_\alpha f_a \tag{23}$$

$$\rho\mathbf{u} = \sum_\alpha \mathbf{e}_\alpha f_\alpha \tag{24}$$

To solve the Poisson equation with strong nonlinearity, eq 12, we employ another evolution method on the same grid system, the lattice Poisson method (LPM),[24,41] by tracking the electric potential distribution transporting on the discrete lattices. First we extend eq 12 into a time-dependent form

$$\frac{\partial\psi}{\partial t} = \nabla^2\psi + g_s(\mathbf{r}, \psi, t) \tag{25}$$

with $g_s = [1/(\varepsilon\varepsilon_0)]\sum_i z_i e n_{i,\infty} \exp\{[-z_i e/(k_b T)]\psi\}$. Thus, the Poisson equation becomes a Navier−Stokes type PDE with a source term $g_s$ and can be solved numerically by another set of lattice evolution method equations. Because the source term is extremely large near the boundaries, the popular 3D fifteen-speed model (D3Q15) is not stable. We adopt the following discrete evolution equation in the D3Q19 model for electric potential distribution[24,41]

$$g_\alpha(\mathbf{r} + \Delta\mathbf{r}, t + \delta_{t,g}) - g_\alpha(\mathbf{r}, t) = -\frac{1}{\tau_g}[g_\alpha(\mathbf{r}, t) - g_\alpha^{eq}(\mathbf{r}, t)] + \left(1 - \frac{0.5}{\tau_g}\right)\delta_{t,g}\omega_\alpha g_{rhs} \tag{26}$$

where the equilibrium distribution of the electric potential evolution variable $g$ is

$$g_\alpha^{eq} = \begin{cases} 0 & \alpha = 0 \\ \psi/18 & \alpha = 1 \text{ to } 6 \\ \psi/18 & \alpha = 7 \text{ to } 18 \end{cases} \tag{27}$$

The time step for the electric potential evolution is

$$\delta_{t,g} = \frac{\delta_x}{c_g} \tag{28}$$

where $c_g$ is the lattice speed for the electric potential propagation.[41] The dimensionless relaxation time is

$$\tau_g = \frac{9}{5\delta_x c_g} + 0.5 \tag{29}$$

It has been proved that $c_g$ can be any positive number as long as the value of $\tau_g$ is within 0.5 and 2.[41,42] After evolving on the discrete lattices, the macroscopic electric potential can be calculated using

(39) Chen, S.; Doolen, G. D. *Annu. Rev. Fluid Mech.* **1998**, *30*, 329–364.
(40) He, X.; Chen, S.; Doolen, G. D. *J. Comput. Phys.* **1998**, *146*, 282–300.
(41) Wang, J. K.; Wang, M.; Li, Z. X. *Commun. Nonlinear Sci. Numer. Simul.* **2008**, *13*, 575–583.
(42) Wang, J. K.; Wang, M.; Li, Z. X. *Int. J. Therm. Sci.* **2007**, *46*, 228–234.

$$\psi = \sum_{\alpha} (g_{\alpha} + 0.5\delta_{t,g} g_{rhs} \omega_{\alpha}) \tag{30}$$

Such an evolution equation for the electric potential distribution, eq 26, is valid for both steady flows and unsteady flows at very low velocities because the electromagnetic susceptibility effect is neglected. Although the lattice evolution method for the nonlinear Poisson equation is not as efficient as the multigrid solutions for simple geometries because of its long wavelength limit, it is more suitable for parallel computing and for geometrical complexity.[43,44]

*Boundary Condition Treatments.* The boundary condition implementations are critical to the accuracy of the numerical simulations. The hydrodynamic boundary conditions for the LBM have been studied extensively.[45−48] The conventional bounce-back rule is the most commonly used method to treat the velocity boundary condition at the solid-fluid interface because of its easy implementation, where momentum from an incoming fluid particle is simply bounced back in the opposite direction as it hits the wall.[39] However, the conventional bounce-back rule has two main disadvantages. First, it requires the dimensionless relaxation time strictly within the range of (0.5, 2), otherwise the prediction will deviate from the correct result.[45] Second, the non-slip boundary implemented by the conventional bounce-back rule is not exactly located at the boundary nodes, which will lead to inconsistencies when the LBM is coupled with other PDE solvers on the same grid set.[48] To overcome the inconsistencies between the LBM and other PDE solvers on the same grid set, one can replace the bounce-back rule with another "non-slip" boundary treatment, such as the one proposed by Inamuro et al.,[46] with the cost of losing the easy implementation for complicated geometries. An alternative solution is to modify the boundary condition treatments of the PDE solver for the electric potential distribution to be consistent with the LBM with the conventional bounce-back rule.

In this contribution, the bounce-back rule for the non-equilibrium distribution proposed by Zou and He[47] is extended to both hydrodynamic and electrodynamic boundary treatments to deal with the complex geometries of random roughness.

At the boundary the following hydrodynamic condition holds:

$$f_{\alpha}^{neq} = f_{\beta}^{neq} \tag{31}$$

where the subscripts α and $\beta$ represent the opposite directions.

Analogously, the non-equilibrium "bounce-back" rule for the electric potential distribution at the wall surfaces is suggested as

$$g_{\alpha}^{neq} = -g_{\beta}^{neq} \tag{32}$$

These boundary treatments are easy to implement for complicated geometries and have approximately second-order accuracy.[47,48]

## RESULTS AND DISCUSSION

We consider the electrokinetic flows in a 3D charged rough microchannel. The 3D roughness is generated by the algorithm described in section 3.1. The solid surfaces are homogeneously charged with a zeta potential, $\zeta$, and the electrolyte solution is driven to flow through the channel by an external electric field (**E**) along the $x$ direction.

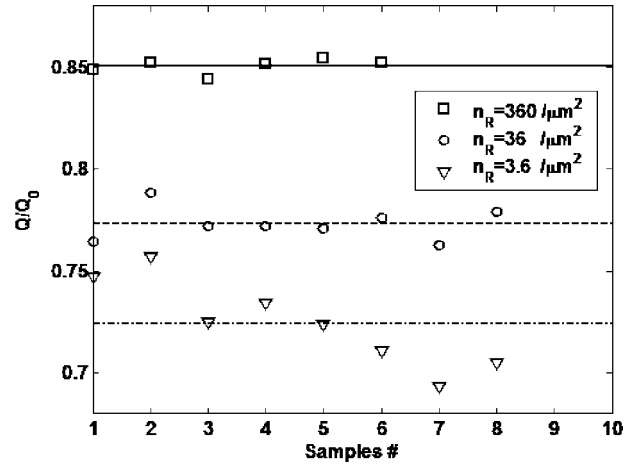


**Figure 2.** Flow rate for three roughness number densities. The symbols are simulated results for different samples, and the lines represent the statistical average values for each case, where $V_R$ = 0.05 and $\lambda/H$ = 0.1683 with $\lambda$ representing the Debye length.

In the present simulations, the channel width $H$, defined as the distance between the two original smooth base walls, is fixed at one micron. A $60 \times 60 \times 60$ uniform cubic grid is used. Periodic boundary conditions are implemented in the $x$ and $y$ directions. We change the values of the generation parameters ($s_d$, $D_i$ and $V_R$) to vary the geometries of roughness. The bulk ionic concentration $n_\infty$ is $0.3 \times 10^{-5}$ M for most cases and is varied from 0.3 to $3.3 \times 10^{-5}$ M when the Debye length needs to be changed. Other properties and parameters used in this work are as follows: the fluid density $\rho = 999.9$ kg/m$^3$, the dielectric constant $\varepsilon_r\varepsilon_0 = 6.95 \times 10^{-10}$ C$^2$/J m, the dynamic viscosity $\mu$ = 0.889 mPa s, the temperature $T$ = 273 K, the surface zeta potential −50 mV, and the external electric field strength $E = 1 \times 10^6$ V/m. The electroosmotic flow considered in this contribution is very slow and the Reynolds number is on the order of $10^{-3}$−$10^{-5}$.

**Effect of Roughness Number Density.** First we consider the effects of the roughness number density $n_R$ for a given total roughness volume fraction ($V_R$ = 0.05). The roughness elements are assumed to be isotropic. The roughness number density is changed through the value of the roughness distribution probability $s_d$, with the corresponding $n_R$ calculated by eq 13a.

Figure 2 shows the dimensionless flow rate for three different roughness number density cases. The volume flow rate, $Q$, for the incompressible fluid is calculated by

$$Q = \int u_x \, \mathrm{d}A \tag{33}$$

where $u_x$ is the velocity in $x$ direction (same as the direction of $E$) and $A$ the area of cross section. $Q_0$ is the volume flow rate for the original smooth channel with all the same conditions. For all the three cases, the total volume fraction of roughness is 0.05, and the bulk ionic concentration is $0.3 \times 10^{-5}$ M.

Since the generated structure of roughness is random, the calculated flow rates do not fall into the same value even for the


(43) Kang, Q. J.; Zhang, D. X.; Chen, S. Y. *Phys. Rev. E* **2002**, *66*, 056307.
(44) Kang, Q. J.; Lichtner, P. C.; Zhang, D. X. *J. Geophys. Res.* **2006**, *111*, B05203.
(45) Noble, D. R.; Chen, S. Y.; Georgiadis, J. G.; Buckius, R. O. *Phys. Fluids* **1995**, *7*, 203–209.
(46) Inamuro, T.; Yoshino, M.; Ogino, F. *Phys. Fluids* **1995**, *7*, 2928–2930.
(47) Zou, Q. S.; He, X. Y. *Phys. Fluids* **1997**, *9*, 1591–1598.
(48) Rohde, M.; Kandhai, D.; Derksen, J. J.; Van den Akker, H. E. A. *Phys. Rev. E* **2003**, *67*, 066703.

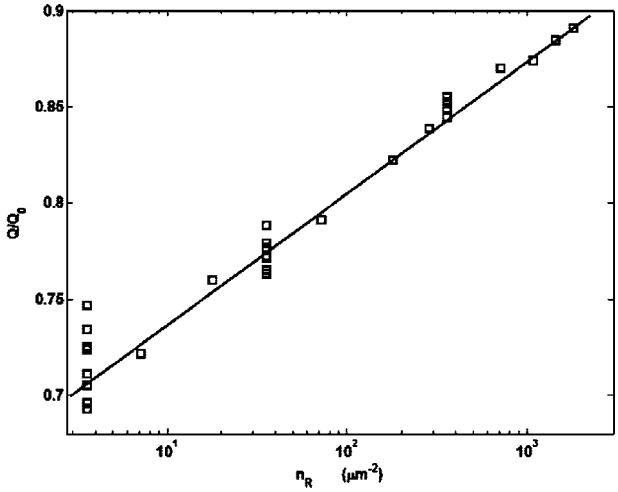


**Figure 3.** Electroosmotic flow rate versus roughness number density. The symbols are the simulated results, and the solid line is a linear fit. $V_R = 0.05$ and $\lambda/H = 0.1683$.

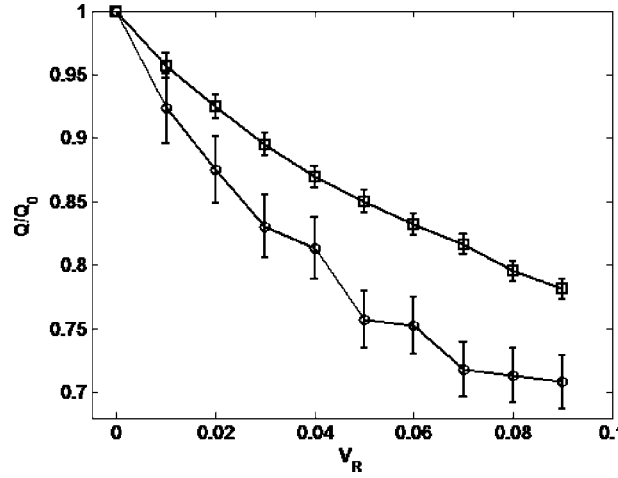


**Figure 4.** Electroosmotic flow rates versus total roughness volume fraction. The squares are results for $n_R = 360/\mu m^2$ with 1% error bars and the circles are those for $n_R = 36/\mu m^2$ with 3% error bars.

same set of parameters but fluctuate around the statistical average. Figure 2 indicates that the fluctuation decreases as the roughness number density increases for a given total roughness volume fraction. For the current three cases with finite samples, the fluctuation is greater than 6% for $n_R = 3.6/\mu m^2$ ($s_d = 0.001$), around 3% for $n_R = 36/\mu m^2$ ($s_d = 0.01$), and less than 1% for $n_R = 360/\mu m^2$ ($s_d = 0.1$).

Figure 3 shows the calculated dimensionless electroosmotic flow rates when the roughness number density varies from 3.6 to 1800 $/\mu m^2$, where the total volume fraction of roughness is 0.05 and the bulk ionic concentration $n_\infty$ is $0.3 \times 10^{-5}$ M. The flow rate increases with the roughness number density. When a logarithmic scale is used for the $x$ axis, the flow rate appears to increase linearly. In other words, the flow rate increases with the roughness number density nearly logarithmically.

**Effect of Roughness Volume Fraction.** For the given roughness number density ($n_R$) and anisotropy parameters ($D_i$), the total roughness volume directly influences the size of roughness elements and therefore the resistance of the channel flow. Figure 4 shows the flow rates when the roughness total volume fraction is changing from 0.01 to 0.09 for two given roughness number densities, where $n_\infty = 0.3 \times 10^{-5}$ M. There are 1% fluctuation error bars for $n_R = 360/\mu m^2$ ($s_d = 0.1$) and 3% fluctuations for $n_R = 36/\mu m^2$ ($s_d = 0.01$). For both cases, the flow rate decreases with the roughness total volume fraction. The flow rate difference between the two roughness number densities increases with the roughness volume fraction in the current volume fraction range (0.01∼0.09).

**Anisotropy Effect.** So far the roughness elements considered are statistically isotropic. In this section we investigate the anisotropy effect of the roughness elements. As mentioned above, the anisotropy of the roughness geometry can be controlled by the directional growth probabilities, and the ratio rather than the absolute values of $D_j$ plays the key role in determining the anisotropy. The directional characteristic length is proportional to the square root of the corresponding directional growth probability. To make the anisotropy effects easily understood, we keep the other two directional growth probabilities equal when changing the concerned one. For example, when we

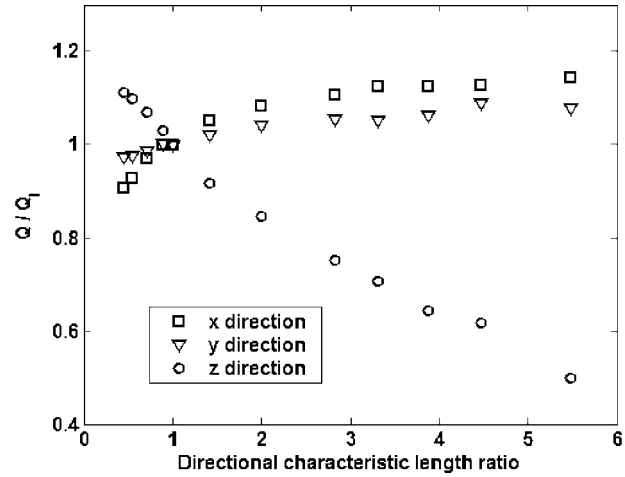


**Figure 5.** Anisotropic geometry effects on electroosmotic flow rate for different directional characteristic length ratios, where $n_R = 36/\mu m^2$ ($s_d = 0.01$), $V_R = 0.05$ and $\lambda/H = 0.1683$.

consider the $y$ directional anisotropy effect, we keep $D_x:D_y:D_z = 1:L_y^2:1$ and change the value of $L_y^2$. For such a case, $L_y$ will be the value of $x$ axis for $y$ directional characteristic length ratio in Figure 5.

Figure 5 shows the normalized flow rates for different anisotropy characteristics for the given roughness number density ($n_R = 36/\mu m^2$) and roughness volume fraction ($V_R = 0.05$), where $Q_i$ denotes the volume flow rate for the isotropic roughness geometry. The $x$ axis denotes the specified directional characteristic length ratio to the other two, which could be $L_x$, $L_y$, or $L_z$. The result indicates that, first of all, the flow rate varies with the directional anisotropy monotonically for all the three directions. The flow rate decreases with the $z$-directional characteristic length (roughness height), but increases with both $x$-directional length (roughness length) and $y$-directional length (roughness width). For the current geometric parameters and electrolyte properties, (1) compared with the isotropic structure case, that is, the ratio equals unity, the flow rate will be lower once the roughness height ($z$ length) is larger; otherwise the flow rate will be higher; (2) the increase in

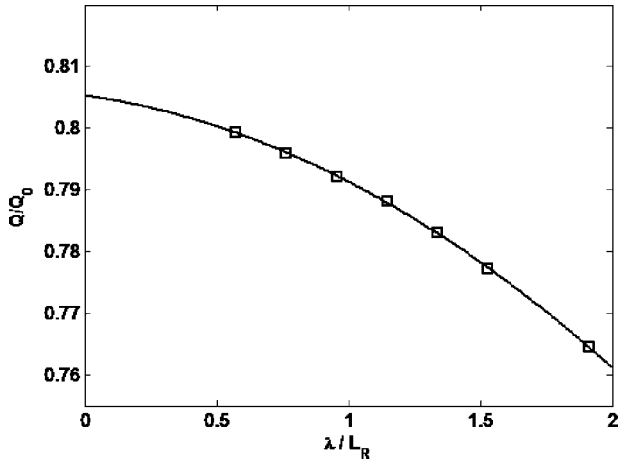


**Figure 6.** Dimensionless electroosmotic flow rate for different Debye length. The symbols are the simulation results, while the line is the quadratic fitting curve.

roughness length (the flow direction) will enhance the flow rate more than that in roughness width.

**Effect of the Debye Length.** Theoretical studies on electroosmotic flows in rough channels have been reported for both thin and thick double layers.[28] However, it is challenging to do similar analyses when the Debye length is comparable to the characteristic length of roughness because the linear assumptions are not valid any more. Using our numerical framework, the Debye length effects on the electroosmotic flows in rough microchannels have been investigated when the Debye length is close to the roughness size.

We have generated the microstructure of a rough microchannel with the parameters: $s_d = 0.01$, $D_x{:}D_y{:}D_z = 1{:}1{:}1$ and $V_R = 0.05$. The characteristic height of roughness ($L_R$) can be then calculated from eq 13b, that is, $L_R = 0.088H$. We change the bulk ionic concentration $n_\infty$ from 3.3 to $0.3 \times 10^{-5}$ M to vary the normalized Debye length ($\lambda/L_R$) from 0.57 to 1.91.

The Debye length effect on the electroosmotic flow rate in a rough microchannel is shown in Figure 6 when the Debye length is around the roughness characteristic length. The flow rate is normalized by the flow rate in the corresponding original smooth channel at the same ionic concentration, $Q_0$. The result indicates that the normalized electroosmotic flow rate decreases with the Debye length monotonically. The solid line in Figure 6 is the quadratic fitting curve for the simulation results. From this curve, when the Debye length ($\lambda$) is much smaller than the roughness characteristic length ($L_R$), that is, $\lambda/L_R \ll 1$, the flow rate in the rough microchannel is still lower than that in the corresponding original smooth microchannel ($Q \approx 0.805Q_0$). This result is inconsistent with the theoretical prediction for the large scale channel flows with the thin Debye layer assumption,[49,50] which concludes that the flow rate ratio should approach 1 for small values of the Debye length. The reason may lie in that in the microchannel the roughness occupies much more volume fraction and causes larger shape resistance than those in the large scale channel, even though the absolute size of roughness elements might be similar.

(49) Morrison, F. A. *J. Colloid Interface Sci.* **1970**, *34*, 210–214.
(50) Morrison, F. A. *J. Colloid Interface Sci.* **1971**, *36*, 139–145.

**Effects of the Shape Resistance.** To find out whether the shape resistance is the main reason for the electroosmotic flow rate reduction in rough microchannels even at very small Debye length, we simulate the Poiseuille flows driven by a pressure gradient in both the given rough channel and its original smooth channel, and then compare the velocity profiles. We use the Poiseuille flow because we can compare the results with the theoretical solutions. The same rough channel used in Figure 6 is adopted here. We fit the averaged velocities of the bulk flow to a parabolic form. The viscosity can be obtained from the fitting parabolic relationship. This process can be found in the Supporting Information, section S-1. It has been found that the roughness does not influence the viscosity of the fluid but only *extends* the walls into the fluid by some distance. This effect caused by the shape resistance of roughness certainly decreases the flow rate in the electroosmotic flows in rough microchannels. From the fitted parabolic curve we can determine the effective smooth channel width ($H_e$) and hence the effective wall extension length ($L_w$) for the rough channel. The values of $H_e$ and $L_w$ depend on the roughness shape, size, and number density as well. For the current case ($s_d = 0.01$, $V_R = 0.05$ and isotropic roughness elements) the effective wall extension length ($L_w$) is approximately equal to the roughness averaged height ($L_R$), that is, $H_e \approx H - 2L_R$.

We then compute the electroosmotic flow rates for both the rough channel ($Q$), the original smooth channel ($Q_0$), and the effective smooth channel ($Q_e$) for seven different conditions shown in Figure 6. The effective smooth channel width $H_e = H - 2L_R$ is used. We find that the relative errors between $Q_e$ and $Q_0$ are larger than 25% but the relative errors between $Q_e$ and $Q$ are less than 3%, which is on the same order of errors introduced by the randomness of the roughness structure. The detail data can be found in the Supporting Information, section S-2. This result indicates that it is the shape resistance of roughness that reduces significantly the flow rate in the rough microchannel compared with that in the original smooth channel, and that makes the flow rate ratio less than 1 even for the case of a thin Debye layer. The inconsistence with the conventional theoretical analysis in rough channel with the thin Debye layer assumption[50] lies in that the relative size of roughness in microchannels is much larger than that in large channels even if the absolute size of roughness is similar. The shape resistance in rough microchannels therefore has much stronger effect than in the large channels and reduces the electroosmotic flow rate significantly.

## CONCLUSIONS

In this contribution, we presented a numerical framework to model the electrokinetic transport in microchannels with random roughness. The 3D microstructure of the rough channel is generated by a random generation-growth method with three statistical parameters to control the geometric characteristics of the roughness. The governing equations for the electrokinetic transport are then solved by a high-efficiency lattice Poisson–Boltzmann method in the complex geometries.

The electrokinetic transport in the rough channel is greatly influenced by the geometric characteristics of the roughness. For a given total volume fraction of roughness elements, a higher number density not only results in a higher electroosmotic flow

rate through the channel but also leads to a lower fluctuation because of the randomness. The electroosmotic flow rate increases with the roughness number density nearly logarithmically for a given volume fraction of roughness but decreases with the volume fraction of roughness for a given roughness number density. For both given volume fraction and number density of roughness, the electroosmotic flow rate is enhanced by the increase in roughness length and width or the decrease in roughness height. For a given microstructure of rough microchannel, the electroosmotic flow rate decreases with the Debye length. The shape resistance of roughness plays an important role in microchannel flows leading to an electroosmotic flow rate lower than that in the original smooth channel even for a very thin double layer.


## ACKNOWLEDGMENT

This work is supported by LANL's LDRD Project 20080727PRD2, through the J. R. Oppenheimer Fellowship awarded to M.W. The authors would like to thank Prof. T. M. Squires, Dr. J. K. Wang, Prof. J. G. Santiago, and Prof. D. Q. Li for helpful discussions.


## SUPPORTING INFORMATION AVAILABLE

Further details are given in sections S-1 and S-2. This material is available free of charge via the Internet at http://pubs.acs.org.


Received for review December 4, 2008. Accepted March 6, 2009.

AC802569N